Unraveling the Role of Metal-Support Interactions on the Structure Sensitivity of Fischer-Tropsch Synthesis

THE JOURNAL OF PHYSICAL CHEMISTRY C
A JOURNAL OF THE AMERICAN CHEMICAL SOCIETY

pubs.acs.org/JPCC

Article

Unraveling the Role of Metal−Support Interactions on the Structure Sensitivity of Fischer−Tropsch Synthesis

Michel P. C. Van Etten, Michelle E. De Laat, Emiel J. M. Hensen, and Ivo A. W. Filot*

Cite This: *J. Phys. Chem. C* 2023, 127, 15148−15156

Read Online

ACCESS | Metrics & More | Article Recommendations | Supporting Information

ABSTRACT: Structure sensitivity plays a pivotal role in heterogeneous catalysis and the Fischer−Tropsch reaction is one of the prime examples of such a structure-sensitive reaction. The activity and selectivity of this reaction depend on the size of the nanoparticle and this trend is observed for a whole range of support materials. To understand why metal−support interactions do not affect this trend, a ReaxFF force field is developed that effectively mimics the broad variety of support materials and captures the metal−support interaction strength into a single structural parameter. Particles of 1−9 nm embedded on support materials are sampled using simulated annealing molecular dynamics and the effect of the metal−support interaction on the active site distribution is studied. It is found that although the size-dependency profile of various active site topologies depends on the interaction strength of the nanoparticle with the support, step-edge sites with an FCC(110) motif remain insensitive to the type of support. Based on microkinetic simulations, it is established that these sites are predominantly responsible for the observed atom-based FTS activity rationalizing why Fischer−Tropsch synthesis is structure-sensitive but support-insensitive.

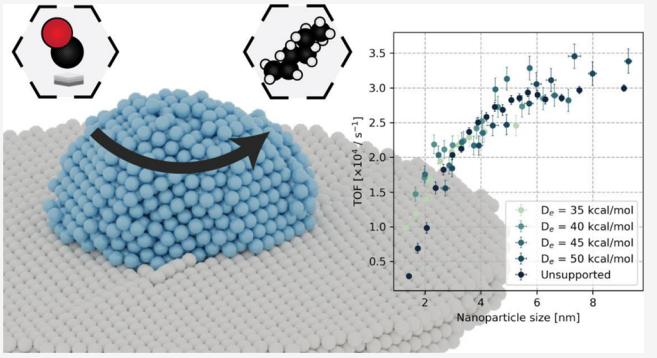

INTRODUCTION

Metallic nanoparticles are used extensively as heterogeneous catalysts in the chemical industry. These nanoparticles are several nanometers in size and expose a variety of active site configurations such as steps, kinks, edges, and corners. Almost a century ago, Taylor already suggested that these coordinatively unsaturated groups of atoms can act as adsorption sites where reactants bind temporarily and where chemical transformations are promoted.[1] Building on this concept, Boudart further classified reactions based on whether the catalyst activity depends on the dispersion of the catalyst material, giving rise to the terminology of structure-sensitive and structure-insensitive reactions.[2,3] The modern view is that structure sensitivity is caused by the abundance of important active sites as function of the particle size. Examples of structure-sensitive reactions are steam-methane reforming,[4−6] ammonia synthesis,[7−10] and Fischer−Tropsch synthesis.[11−16] For these reactions, the activity depends on the availability of a specific active site that facilitates a low barrier for an otherwise difficult to activate chemical bond. To illustrate, steam-methane reforming requires the activation of C−H σ-bonds which are facilitated by kink and edge sites. Such sites are exposed in greater abundance for smaller nanoparticles. Hence, an increase in the atom-based catalytic activity is observed with decreasing particle size. In contrast, the activity in ammonia and Fischer−Tropsch synthesis depends on the efficiency of the scission of π-bonds in N_2 and CO, respectively, requiring the availability of step-edge sites.[17] It is hypothesized that larger metal particles expose more of such step-edge sites and thus an increase in the atom-based catalytic activity is observed with increasing particle size. This hypothesis is supported by various experimental[8,18,19] as well as theoretical studies.[20−23] Ensuring the optimization of the nanoparticle size is imperative for industrial applications.[24] The utilization of too small nanoparticles leads to the generation of undesirable methane and a loss in activity,[11,25] while excessively large particles fail to effectively utilize the abundant cobalt atoms, thereby rendering catalyst production needlessly costly.

Multiscale modeling is utilized in computational modeling procedures to predict structure sensitivity trends in heterogeneous catalysis.[26] At the atomistic scale, density functional theory (DFT) simulations together with kinetic simulations such as microkinetic modeling (MKM) and kinetic Monte-Carlo are used to identify the reactivity patterns of the active sites exposed by the catalyst. These studies can be linked to mesoscale studies where the abundance of these active sites is

Received: April 4, 2023
Revised: July 12, 2023
Published: August 1, 2023

https://doi.org/10.1021/acs.jpcc.3c02240
J. Phys. Chem. C 2023, 127, 15148−15156

studied as a function of the nanoparticle size. For small nanoparticles less than 2 nm in size, ab initio molecular dynamics is an accurate and suitable method. However, for larger nanoparticles, these methods become computationally intractable. To overcome this issue, empirical force fields provide an alternative that comes at a fraction of the computational cost of ab initio methods. This allows for the study of systems several orders larger in size than what is possible with density functional theory.[27] These empirical force fields typically display a reduced accuracy when transferred from one system to another and as such require (re-)parametrization to exhibit sufficient chemical accuracy comparable to ab initio type of calculations.[28]

Recently, we have conducted a multiscale study of the Fischer−Tropsch reaction wherein DFT, MKM, and molecular dynamics (MD) simulations based on a ReaxFF force field were combined to elucidate the experimentally observed structure sensitivity in Fischer−Tropsch synthesis.[20] We showed that step-edge sites exhibiting an FCC(110) topology were identified to be the locus of the chemical transformation. These steps are stabilized by the formation of nano-islands, whose abundance depends on the size of the nanoparticle. One aspect that was however not explicitly considered in this earlier study is the influence of the support material used to maintain the active phase in the nanoparticle form. Industrially used Co nanoparticles are commonly supported on oxides such as alumina (Al_2O_3), silica (SiO_2), and titania (TiO_2).[29,30] Other oxidic supports such as MgO[31,32] and CeO_2[33,34] have been studied as well. The primary functions of these materials are to disperse the active metal, stabilize the nanoparticles at elevated temperatures, and provide mechanical strength.[35] The textural properties of the support greatly affect the dispersion of the catalyst nanoparticles and control their size and morphology. For example, strong metal−support interactions can result in the formation of so-called "pancake"-shaped catalysts, whereas weak metal−support interactions give rise to more spherically shaped catalysts. It is reasonable to infer that nanoparticles with varying shapes will exhibit distinct active site abundancies since the shape determines the type of facets that are exposed.[36]

In this study, we aim to understand how the support can modulate the shape and size of the nanoparticle. Although the Fischer−Tropsch reaction is known to be a structure-sensitive reaction, it is observed that metal−support interactions do not affect the overall trend.[37] This raises the question why the support plays no other role than the modulation of the particle size and what causes the Fischer−Tropsch reaction to be shape-insensitive. To answer this question, we have developed a ReaxFF force field that effectively mimics the broad variety of support materials and captures the metal−support interaction strength via the bond strength parameter D_e.[38] Conventionally, this single parameter is used to describe the energy gained upon formation of a chemical bond as function of the bond order. We have generalized this to describe the interaction between a Co atom in the nanoparticle and an atom of the support. Variation of this D_e parameter allows then for describing the interaction strength of different surfaces. Extensive molecular dynamics simulations are conducted to study the dispersion, particle size, and active site abundance as function of the structural parameter. In turn, the surface abundance of specific active sites is then used in a microkinetic model to predict the FTS activity as a function of the particle size and the metal−support interaction strength. Herein, the experimentally observed structure sensitivity is reproduced. Importantly, it is found that although the support modulates the shape of the nanoparticle yielding different structure sensitivity trends for a variety of active sites, the structure sensitivity of active sites that facilitate efficient C−O bond scission is insensitive to the metal−support interaction strength.

METHODS

Interaction Model. In order to explore the cobalt nanoparticle geometry as a function of size and cobalt−support interaction strength, we employed simulated annealing molecular dynamics (MD) simulations based on a reactive force field.[27,38,39] To assess the impact of the interaction strength between the metal and the support, we introduced a hypothetical support possessing an FCC crystal structure, despite the absence of such a crystal structure in any of the refractory oxides. This approach allowed us to isolate the effect of the metal−support interaction strength, independent of any influence stemming from the crystal packing of the support. It is worth noting that this approach incurs the trade-off of neglecting any effects directly attributable to the local topology of the support.

Although there exists a multitude of generalized force fields in the literature, we here opted to use the previously trained and validated ReaxFF force field atomic parameters for cobalt[20] as a starting point for describing the atomic parameters of the support. This specific force field was trained to accurately describe Co nanoparticles and facilitates a straightforward yet effective description of the bonding strength between the support and the Co atoms by means of a single (σ-bond) dissociation parameter (D_e). This dissociation energy D_e is used to calculate the bond energies (E_{bond}) as given by the following equation.

$$E_{bond} = -D_e \cdot BO_{ij} \cdot \exp(p_{be1}(1 - (BO_{ij})^{p_{be2}})) \quad (1)$$

Herein, BO_{ij} is the bond order between atoms i and j and p_{be1} and p_{be2} are the bond parameters.[38] In this study, D_e was varied between 35−50 kcal/mol. A detailed overview of the reactive force field parameters can be found in Tables S1−S3.

MD Simulation Settings. The canonical ensemble (NVT) using the velocity Verlet algorithm with a time step of 0.25 fs was used to perform the MD simulations. The temperature of the system was controlled by the Nosé−Hoover thermostat with a temperature damping constant of 100 fs. All MD simulations were executed using the AMS software suite.[40] For simulated annealing, the cobalt atoms were initially positioned in a simple cubic crystal structure to prevent bias toward the final bulk structure. The cubic structure of cobalt atoms was placed in the center of the periodic unit cell on top of the four-layered support with an FCC(111) orientation at a distance of 2.5 Å. To avoid spurious interactions of the nanoparticle with neighboring super cells, a periodic unit cell was used to accommodate a support which has dimensions in the x- and y-directions that are at least twice as large as compared to the diameter of the nanoparticle. For each of the simulations, no cobalt atoms were observed that moved across the periodic boundaries. For each set of simulated systems with a constant number of cobalt atoms and constant cobalt−support interaction strength, 40 simulations were performed for proper statistical sampling. To this purpose, the initial velocities of all atoms were randomly generated from a Gaussian distribution

https://doi.org/10.1021/acs.jpcc.3c02240
J. Phys. Chem. C 2023, 127, 15148−15156

Table 1. Adsorption Energies of a Single Co Atom on the Various Supports from the DFT Calculations and the ReaxFF Parameter D_e Derived by Using Eqs 2−7

	Co(111)	Co(100)	MgO(100)	SiO_2(100)	Al_2O_3(001)	TiO_2(110) (rutile)	CeO_2(111)
DFT (kJ/mol)	−578	−626	−132	−213	−281	−367	−417
D_e (kcal/mol)	53.6	55.5	36.2	39.4	42.0	45.4	47.3

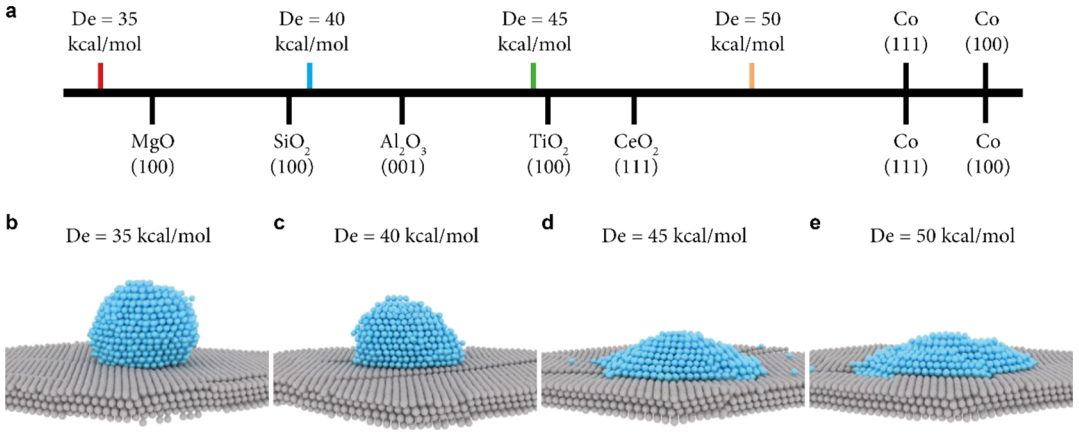

Figure 1. (a) Schematic overview of the adjusted MD single-atom adsorption energies (above the horizontal line) of the simulated cobalt−support interaction strengths and DFT single-atom adsorption energies (below the horizontal line) on a variety of supports; (b−e) visualization of representative supported cobalt nanoparticles of 1728 atoms for D_e values of (b) 35 kcal/mol, (c) 40 kcal/mol, (d) 45 kcal/mol, and (e) 50 kcal/mol.

with a variance k_BT/m using the Mersenne Twister pseudorandom number generator.[41] For each of the simulations, the simulated annealing trajectory of 110 ps consisted of a relatively long initialization period of 50 ps and an annealing period of 60 ps. During the initialization period, the temperature of the system was kept constant at 1500 K. During the annealing period, the temperature of the system was slowly cooled to 300 K by decreasing the temperature of the system in steps of 100 K at 5 ps intervals.[20]

For each simulation, it was furthermore verified that prolonging the simulation time did not yield statistically different observables. For example, MD simulations of 165 and 220 ps were performed for supported cobalt nanoparticles of 512 atoms for the dissociation energy range of 35−50 kcal/mol. The radial distribution functions (RDFs) for each of these four cobalt−support interaction strengths (Figure S1) show that in all cases, the RDFs correspond to those expected for a bulk phase composed of fcc and hcp crystalline cobalt, which is consistent with XRD patterns as found from the experiment.[42,43]

Electronic Structure Calculations. To compare our simulated supported cobalt nanoparticles with different cobalt−support interaction strengths of several typical support materials for cobalt-based Fischer−Tropsch synthesis, quantum-chemical calculations based on spin-polarized density function theory (DFT) were performed for single-atom cobalt on different supports. All DFT calculations were executed using the Vienna Ab Initio Simulations package (VASP) which employs a plane wave approach in conjunction with the projector-augmented wave (PAW) method for describing the interactions between the nuclei and core electrons.[44−47] To describe the electron−electron interactions, the Perdew−Burke−Ernzerhof (PBE) exchange−correlation functional was used.[48] A plane wave basis set with a kinetic energy cutoff of 400 eV was used for the valence electrons. Partial occupancies were determined using a first-order Methfessel−Paxton scheme with a smearing width of 0.2 eV.[49] Electronic convergence was set to 10^{-5} eV and geometries were converged to 10^{-3} eV/Å using the conjugate-gradient algorithm that employs trial and corrector steps to converge both the energy of the structure as well as the forces on the ions. All atoms were allowed to relax. The support layers (3 × 3 supercell) with the adsorbed single-atom cobalt were placed in the center of the unit cell, and a vacuum layer of 15 Å was added perpendicular to the surface to avoid the spurious interactions between the images. The *k*-points for the Brillouin zone sampling were 3 × 3 × 1.

RESULTS AND DISCUSSION

Parameter Establishment. To express the cobalt−support interaction strength for MgO, SiO_2, Al_2O_3, TiO_2, and CeO_2 in terms of the ReaxFF parameter D_e, a procedure based on two control points, corresponding to a single Co atom adsorbed on Co(100) and Co(111), is used as given by eqs 2−7.

$$D_{e,i} = a_1 \cdot E_i^{DFT} + b_1 \tag{2}$$

where $D_{e,i}$ is the ReaxFF parameter D_e for surface *i*, and E_i^{DFT} is the adsorption energy for a single Co atom on surface *i*. The parameters a_1 and b_1 are given by

$$a_1 = \frac{50 - 35}{E'^{ReaxFF}_{D_e=50} - E'^{ReaxFF}_{D_e=35}} \tag{3}$$

and

$$b_1 = 35 - a_1 \cdot E'^{ReaxFF}_{D_e=35} \tag{4}$$

The scaled ReaxFF energies $E_i'^{ReaxFF}$ are calculated by

$$E_i'^{ReaxFF} = a_2 \cdot E_i^{ReaxFF} + b_2 \tag{5}$$

Herein, the parameters a_2 and b_2 are given by

https://doi.org/10.1021/acs.jpcc.3c02240
J. Phys. Chem. C 2023, 127, 15148−15156

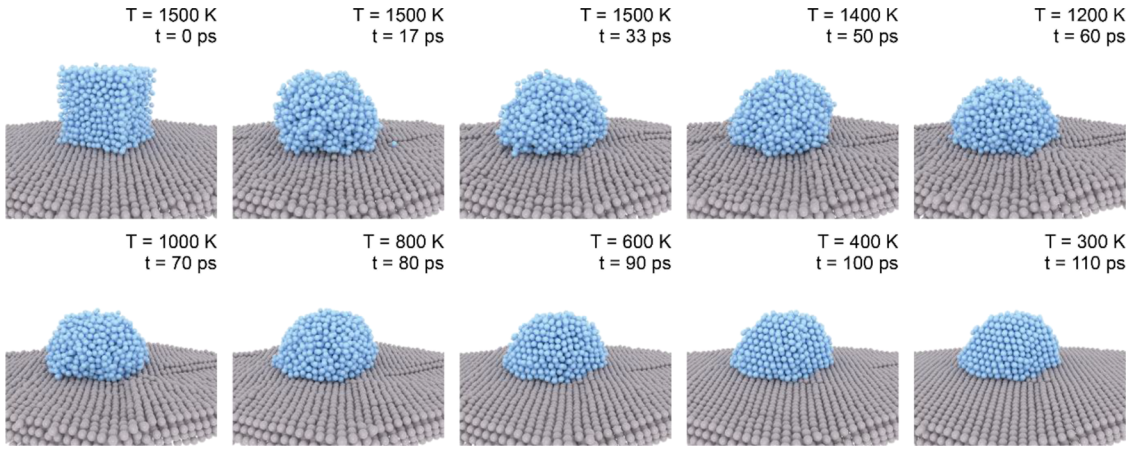

Figure 2. Snapshots of a MD trajectory of a supported cobalt nanoparticle of around 4 nm with a cobalt−support interaction of 40 kcal/mol.

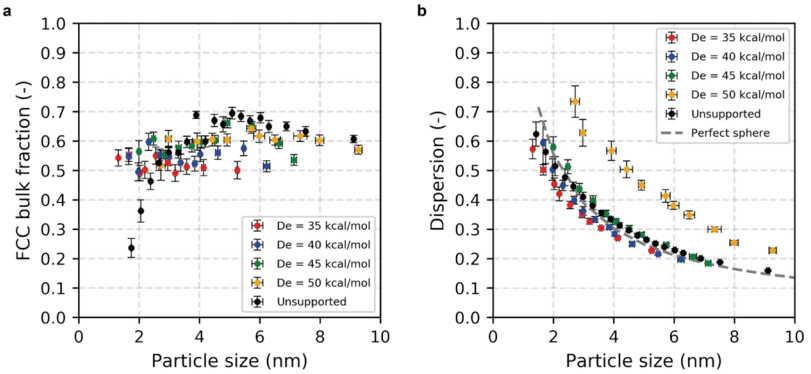

Figure 3. Average FCC bulk fraction (a) and dispersion (b) for supported cobalt nanoparticles with the metal−support interaction strength of (red) 35 kcal/mol, (blue) 40 kcal/mol, (green) 45 kcal/mol, and (orange) 50 kcal/mol, and (black) unsupported cobalt nanoparticles. Error bars correspond to the 95% confidence intervals ($\mu \pm \sigma$) as determined by averaging over 40 simulations of particles of the same number of atoms. The dashed gray line in (b) represents the dispersion of a perfectly spherical cobalt nanoparticle.

$$a_2 = \frac{E_{Co(100)}^{DFT/PBE} - E_{Co(111)}^{DFT/PBE}}{E_{Co(100)}^{ReaxFF} - E_{Co(111)}^{ReaxFF}} \quad (6)$$

and

$$b_2 = E_{Co(111)}^{DFT/PBE} - a_2 \cdot E_{Co(111)}^{ReaxFF} \quad (7)$$

where the labels in $E_{Co(100)}^{DFT/PBE}$, $E_{Co(111)}^{DFT/PBE}$, $E_{Co(100)}^{ReaxFF}$, and $E_{Co(111)}^{ReaxFF}$ correspond to the adsorption energies calculated from either DFT or ReaxFF and correspond to adsorption on either a Co(100) or Co(111) surface. For all oxidic supports, we have chosen the most stable surface termination which corresponds to (100) for MgO[50] and SiO_2,[51] (110) for rutile-TiO_2,[52] (001) for Al_2O_3,[53] and (111) for CeO_2.[54] Application of these equations to the DFT calculated adsorption energies of a Co atom adsorbed on MgO, SiO_2, Al_2O_3, TiO_2, and CeO_2 leads to the D_e parameters for these cases, as shown in Table 1.

These data show that the range of D_e between 35 and 50 kcal/mol covers the variation in metal−support interactions of the various supports. In addition, Table 1 shows that cobalt has a relatively weak interaction with a MgO support, an intermediate interaction with SiO_2 and Al_2O_3 supports, and a strong interaction with TiO_2 and CeO_2. The increasing cobalt−support interaction strength trend of MgO > SiO_2 > Al_2O_3 > TiO_2 > CeO_2 is in line with the work of Das and Deo who studied with XRD the crystallite size of Co nanoparticles as function for a broad range of support materials.[55]

Molecular Dynamics. To study the effect of the interaction strength with the support, simulated annealing molecular dynamics simulations were performed. Figure 1b−e shows the resulting supported cobalt nanoparticles as function of the cobalt−support interaction strength. For a weak cobalt−support interaction (35 kcal/mol), an almost spherical cobalt nanoparticle is obtained, which becomes hemispherical for an intermediate cobalt−support interaction (40 kcal/mol) and with further increase of the interaction strength more pancake-like for strong cobalt−support interactions (45−50 kcal/mol). It was found that for D_e values smaller than 35 kcal/mol that the nanoparticle does not adsorb on the support. Larger values, on the other hand, i.e., D_e > 50 kcal/mol, give rise to minor intercalations of Co atoms into the support, reconstruction of the support, and the dispersion of the bigger nanoparticle into smaller ones.

A representative example of an MD trajectory of a 4 nm supported cobalt nanoparticle with a cobalt−support interaction strength of 40 kcal/mol is shown in Figure 2. It can be seen that the shape of the particle rapidly changes from the initial cubic configuration into a more hemispherical one with crystal facets appearing as annealing proceeds. Movies corresponding to the simulated annealing trajectories are available in the Supporting Information. The surface site composition and the bulk composition of the resulting supported cobalt nanoparticles were analyzed with the common neighbor analysis (CNA) method, as described in

https://doi.org/10.1021/acs.jpcc.3c02240
J. Phys. Chem. C 2023, 127, 15148−15156

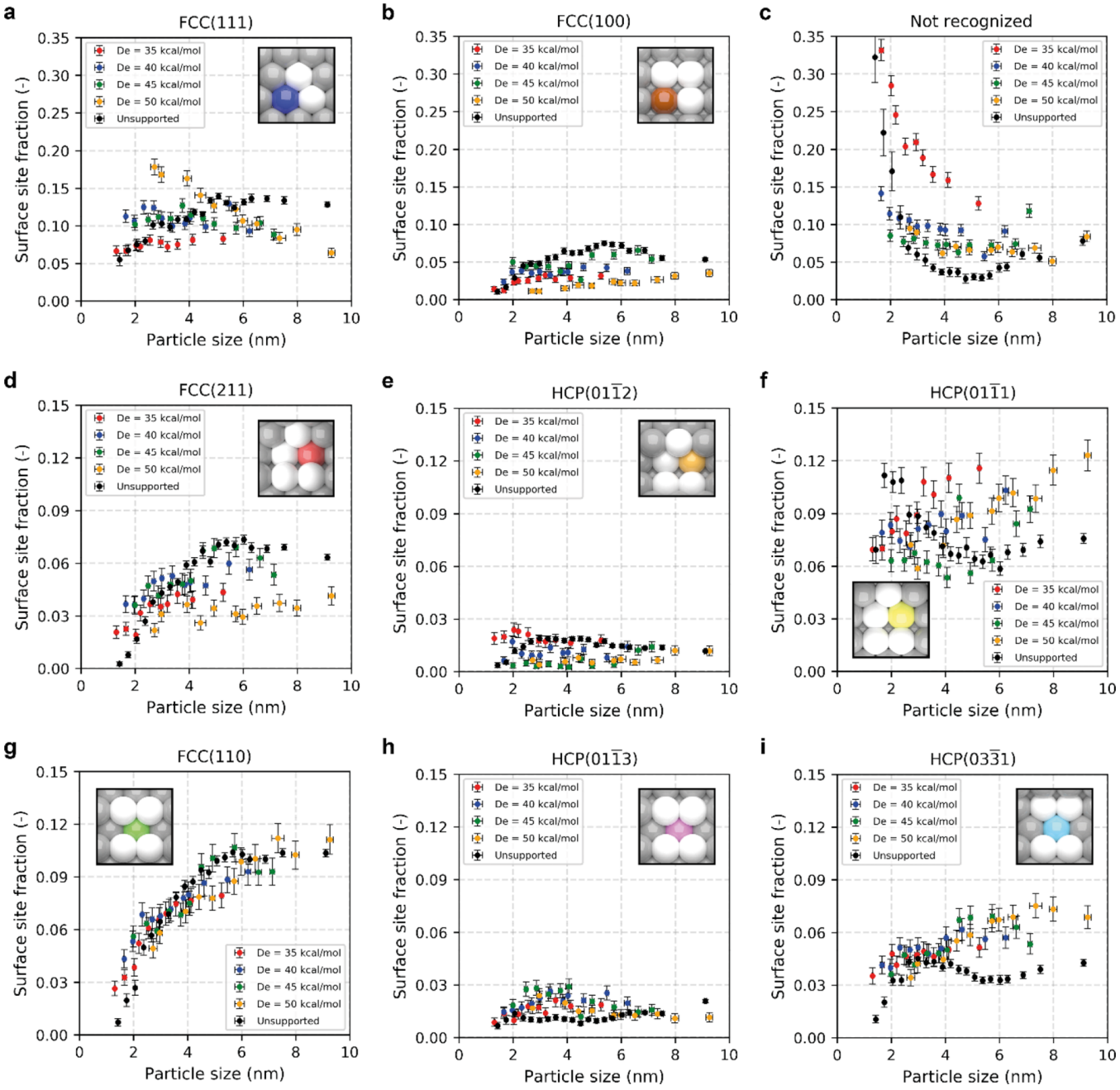

Figure 4. Abundance of terrace sites with (a) FCC(111) and (b) FCC(100) orientation, (c) surface sites not recognized by the CNA algorithm, and abundance of step-edge sites with (d) FCC(211), (e) HCP(01$\bar{1}$2), (f) HCP(01$\bar{1}$1), (g) FCC(110), (h) HCP(01$\bar{1}$3), and (i) HCP(03$\bar{3}$1) orientation, for supported nanoparticles with a metal−support interaction strength of (red) 35 kcal/mol, (blue) 40 kcal/mol, (green) 45 kcal/mol, and (orange) 50 kcal/mol, and (black) unsupported cobalt nanoparticles. Error bars correspond to the 95% confidence intervals determined by averaging over 40 simulations of particles of the same number of atoms. The insets visualize the active site topology wherein the atom used to enumerate the active sites is colored.

our previous work.[20,56,57] A detailed description of the procedure is given in the Supporting Information.

Particle Size, Bulk Composition, and Dispersion. To obtain statistically representative results, we performed 40 independent simulations for each set of systems simulated with a constant number of cobalt atoms and a constant cobalt−support interaction strength. By sampling the particle size, bulk composition, and dispersion in this way, we were able to obtain average values for each system. Table S4 presents the average particle size and standard deviation as a function of the D_e parameter and the number of atoms. Notably, this table indicates that 40 simulations produce sufficiently small standard deviations, enabling the comparison of simulations with different D_e. Additionally, Table S4 indicates that increasing the cobalt−support interaction strength gives rise to larger average particle sizes for a constant number of atoms. This finding is in line with Figure 1b−e, which illustrates that stronger cobalt−support interactions result in higher dispersion of the cobalt atoms over the surface (vide infra).

As shown in Figure 3a, the fraction of bulk atoms, i.e., those atoms that have a coordination number CN ≥ 12, residing in a local environment corresponding to bulk FCC is shown. The

https://doi.org/10.1021/acs.jpcc.3c02240
J. Phys. Chem. C 2023, 127, 15148−15156

FCC bulk fraction is by approximation independent of the particle size for the supported nanoparticles. However, it can be seen that this fraction increases with the particle size for the unsupported particles. This prediction is in line with experimental findings of Kitakami et al. that show that the FCC bulk phase is the dominant phase for nanoparticles below 20 nm.[58] This result is to be expected since the fictitious support exhibits an FCC(111) termination by which a commensurate FCC bulk configuration of the Co nanoparticles is preferred. A stronger cobalt-interaction parameter makes this effect more pronounced.

The average dispersion, as calculated by dividing the number of surface atoms by the total number of atoms, is shown in Figure 3b. The dashed gray line corresponds to the dispersion of perfectly shaped spherical FCC-type nanoparticles in the range of 1.5−10 nm (see the Supporting Information for details). This figure clearly shows that the dispersion increases with increasing cobalt−support interaction strength for similarly sized cobalt nanoparticles. For the weaker cobalt−support interaction strength (D_e = 35 kcal/mol and D_e = 40 kcal/mol; red and blue data points in Figure 3b, respectively), the dispersion is consistently lower than that of ideally shaped spherical nanoparticles (Figure 3b; dashed gray line). In these systems, the cobalt nanoparticles are nearly spherical and have limited interface with the support. Consequently, the bulk phase of the nanoparticles contains a similar number of cobalt atoms to that of ideally shaped spherical particles, while the interaction with the support results in fewer surface atoms. This leads to lower dispersion of these particles compared to ideally shaped spherical particles. We found that the dispersion for the nanoparticles with D_e = 35 and D_e = 40 kcal/mol is on average 14% and 6% lower as compared to the perfectly spherical constructions of the same size. For nanoparticles with a moderate cobalt−support interaction strength, the shape becomes more hemispherical and the dispersion is roughly 9% higher as compared to ideally shaped cobalt nanoparticles of the same size. For weak to moderately interacting supports, it is thus found that the support effect on the dispersion is relatively small. Further increasing the interaction strength to D_e = 50 kcal/mol yields, however, a profound change in the shape and dispersion of the supported cobalt nanoparticles. For high cobalt−support interaction strengths, particles assume a pancake-like shape, with a lower proportion of bulk atoms compared to moderate interaction strengths. The increased surface area of these particles results in greater dispersion, with an average increase of 72% compared to same-sized spherical particles that have a greater proportion of bulk atoms.

Surfaces Site Composition. The activity and selectivity of a catalytic nanoparticle is in part determined by the abundance of specific arrangements of surface atoms. Active sites are pockets of several surface atoms and thus a pattern recognition algorithm is required that is capable of enumerating specific topological arrangements of these surface metal atoms. Here, the common neighbor analysis (CNA) approach is used for the active site recognition.[56,57] Figure 4 shows how the surface abundance of active sites changes with the nanoparticle size and cobalt−support interaction strength. The abundance of terrace sites with an FCC(111) orientation (Figure 4a) is constant for the whole size range for each of the simulated cobalt−support interaction strengths, except for the strongest cobalt−support interaction strength, where the abundance is decreasing with the particle size. Terrace sites with an FCC(100) orientation (Figure 4b) show a lower abundance for the supported nanoparticles as compared to the unsupported cobalt nanoparticles. As function of the particle size for the supported systems, the abundance of the FCC(100) sites remains fairly constant over the whole size range, irrespective of the cobalt−support interaction strength. For each of the simulated cobalt−support interaction strengths, step-edge sites with an FCC(211) orientation (Figure 4d) show a similar trend as that of unsupported cobalt nanoparticles. Herein, a small increase as function of the particle size is observed between approximately 2−4 nm, after which the abundance becomes independent of the particle size. It should be noted that the abundance of FCC(211) sites is significantly lower for supported cobalt nanoparticles with the strongest cobalt−support interaction strength as compared to the other supported and the unsupported systems. Step-edge sites with HCP(01$\bar{1}$2) and HCP(01$\bar{1}$3) orientations (Figure 4e,f) are present in very small amounts over the whole size range for each of the cobalt−support interaction strengths, similar to that of the unsupported cobalt nanoparticles.

No clear trend as function of the metal−support interaction strength is observed for step-edge sites with an HCP(01$\bar{1}$1) orientation (Figure 4f). The abundance of this site varies between around 6% and 12%. The abundance of step-edge sites with FCC(110) and HCP(03$\bar{3}$1) orientation (Figure 4i) increases with size up to ∼6 nm and then levels off for each of the metal−support interaction strengths. In case of FCC(110) step-edge sites (Figure 4g), this trend is similar to that of the unsupported cobalt nanoparticles, while for HCP(03$\bar{3}$1)-orientated step-edge sites (Figure 4i), the point at which the abundance remains constant as function of size was observed at smaller particle sizes for unsupported cobalt nanoparticles as compared to the supported nanoparticles.

Although the CNA algorithm is effective at identifying active sites that adopt a more crystalline configuration, i.e., a packing similar to that observed for bulk FCC or HCP, it behaves relatively poorly for more amorphous structures. Such aberrant topologies are relatively common for the smaller nanoparticles. As can be seen from Figure 4c, the surfaces of smaller particles contain more atoms that cannot be identified by the CNA algorithm. For moderate and strong metal−support interaction strengths, most of these atoms have coordination numbers 5, 6, or 7, which implies that they are edge, corner, and kink atoms. Such low-coordinated sites are usually assumed to be prominent on very small particles and important to C−H bond activation in alkanes. However, they cannot dissociate molecules like CO as relevant to the FT reaction. The surface contribution of such low-coordinated atoms is less than 10% on particles larger than 2.5 nm. It should be mentioned that for a weak metal−support interaction strength (Figure 1b), besides the low-coordinated sites, the atoms that cannot be identified by the CNA algorithm consist of cobalt atoms in a concave site formed at the interface of the cobalt nanoparticle and the support surface.

Kinetic Modeling of Structure Sensitivity Effects. To describe the structure sensitivity of the Fischer−Tropsch reaction, a description beyond the usual Langmuir assumption of a uniform surface is required. Instead, the Taylorian framework in which catalysis occurs by unique active sites that may be present in very small numbers compared to other less active sites is used to describe the surface reactivity of the supported cobalt nanoparticles. The particle-based rate is the sum of rates of a site normalized by its abundance on a particle

https://doi.org/10.1021/acs.jpcc.3c02240
J. Phys. Chem. C 2023, 127, 15148−15156

of a given size and cobalt−support interaction strength. To determine the particle-based rates, we use our previously predicted site-based rates for each of the terrace and step-edge sites identified on cobalt nanoparticles using an extensive microkinetic model under static surface assumptions based on DFT-computed reaction energetics and in which coverage effects are included in the microkinetic model by means of lateral interactions.[20]

The estimated particle-based rates are presented as surface atom-based turnover frequencies (TOFs) in Figure 5. For each

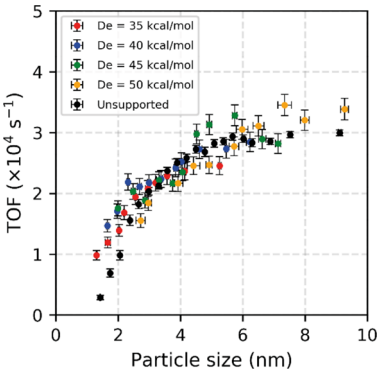

Figure 5. Surface atom-based TOF as a function of the nanoparticle size, for supported nanoparticles with the metal−support interaction strength of (red) 35 kcal/mol, (blue) 40 kcal/mol, (green) 45 kcal/mol, and (orange) 50 kcal/mol, and (black) unsupported cobalt nanoparticles. Error bars correspond to the 95% confidence intervals determined by averaging over 40 simulations of particles of the same number of atoms.

of the simulated cobalt−support interaction strengths, the TOF is low for small particles and increases strongly as a function of the nanoparticle size until a plateau is reached for particles above 5 nm. This structure sensitivity trend is consistent with many experimental observations made for the FT reaction on cobalt for different support materials, as shown in the work of Pestman et al.[37] In our previous work, we concluded that CO conversion for unsupported cobalt nanoparticles is mainly determined by step-edge sites with the FCC(110) orientation. While this active site configuration is clearly size-sensitive, it is observed that it is not shape-sensitive and thus exhibits the same trend irrespective of the cobalt−support interaction strength and whether the nanoparticles are supported or unsupported. By analyzing the contribution of each site to the TOFs (Figure S3, Supporting Information) for each of the supported cobalt nanoparticles, the conclusion remains that CO conversion is mainly determined by step-edge sites with the FCC(110) orientation over the whole simulated particle size and the cobalt−support interaction strength range.

The findings of this study can significantly contribute to the development of optimal Fischer−Tropsch synthesis (FTS) catalyst formulations, providing a more precise understanding of the role of the support. Our findings indicate that the cobalt−support interaction strength should not strongly impact the abundance of active sites as a function of the particle size, provided that all cobalt is reduced. This implies that other parameters such as support texture and thermal conductivity can be further optimized.

CONCLUSIONS

The present work demonstrates an effective procedure for predicting the effect of the metal−support interaction strength on structure sensitivity trends in heterogenous catalysis by identifying catalytic ensembles at the surface of metal nanoparticles obtained by atomistic simulations. Use is made of simulated annealing based on a force field in which the metal−support interaction strength is tuned by varying the ReaxFF parameter corresponding to the dissociation energy for the σ-bond (D_e). To simulate the appropriate cobalt−support interaction strength regime, corresponding to a variety of common support materials for cobalt particles, a D_e range of 35−50 kcal/mol was explored. Through pattern recognition, specific surface atom arrangements corresponding to terrace and step-edge sites are identified and quantified as a function of the particle size and cobalt−support interaction strength. When applied to cobalt particles for catalysis interesting size range between 1 and 9 nm, this approach shows that the density of FCC(110) step-edge sites increases strongly for particle sizes up to around 6 nm and then levels off for larger particles over the whole simulated cobalt−support interaction strength. This trend coincides with the surface-normalized FT activity of these cobalt particles as the FCC(110) sites predominantly determine the CO conversion. As such, in agreement with our previous findings on unsupported cobalt nanoparticles, the conclusion remains that CO conversion is mainly determined by step-edge sites with the FCC(110) orientation over the whole simulated particle size. Importantly, this trend is not affected by the cobalt−support interaction strength. This rationalizes why Fischer−Tropsch synthesis is structure-sensitive, but a shape-insensitive reaction and thus the same structure sensitivity trend are found over a wide range of different support materials.

ASSOCIATED CONTENT

Supporting Information

The Supporting Information is available free of charge at https://pubs.acs.org/doi/10.1021/acs.jpcc.3c02240.

Simulated annealing of supported cobalt nanoparticle (MP4)

ReaxFF parameters; radial distribution functions; particle sizes and standard deviations; fractional contributions to total nanoparticle activity as a function of the particle size; description of the CNA algorithm; and sensitivity analysis of the support atom mass (PDF)

AUTHOR INFORMATION

Corresponding Author

Ivo A. W. Filot − *Laboratory of Inorganic Materials and Catalysis, Department of Chemical Engineering and Chemistry, Eindhoven University of Technology, Eindhoven 5600 MB, The Netherlands;* orcid.org/0000-0003-1403-8379; Email: i.a.w.filot@tue.nl

Authors

Michel P. C. Van Etten − *Laboratory of Inorganic Materials and Catalysis, Department of Chemical Engineering and Chemistry, Eindhoven University of Technology, Eindhoven 5600 MB, The Netherlands*

Michelle E. De Laat − *Laboratory of Inorganic Materials and Catalysis, Department of Chemical Engineering and*

https://doi.org/10.1021/acs.jpcc.3c02240
J. Phys. Chem. C 2023, 127, 15148−15156

Chemistry, Eindhoven University of Technology, Eindhoven 5600 MB, The Netherlands

Emiel J. M. Hensen − *Laboratory of Inorganic Materials and Catalysis, Department of Chemical Engineering and Chemistry, Eindhoven University of Technology, Eindhoven 5600 MB, The Netherlands;* orcid.org/0000-0002-9754-2417

Complete contact information is available at: https://pubs.acs.org/10.1021/acs.jpcc.3c02240

Notes

The authors declare no competing financial interest.

■ ACKNOWLEDGMENTS

This work was supported by the Netherlands Center for Multiscale Catalytic Energy Conversion, and NWO Gravitation program funded by the Ministry of Education, Culture and Science of the government of the Netherlands. The Netherlands Organization for Scientific Research is acknowledged for providing access to computational resources.

■ REFERENCES

(1) Taylor, H. S.; Armstrong, E. F. A Theory of the Catalytic Surface. *Proc. R. Soc. London, Ser. A* **1925**, *108*, 105−111.

(2) Boudart, M., Catalysis by Supported Metals. In *Advances in Catalysis*; Eley, D. D.; Pines, H.; Weisz, P. B., Eds; Academic Press, 1969; vol *20*, pp 153−166.

(3) Boudart, M., *Kinetics of Heterogeneous Catalysis Reactions*; Princeton University Press, 1984.

(4) Ligthart, D. A. J. M.; van Santen, R. A.; Hensen, E. J. M. Influence of Particle Size on the Activity and Stability in Steam Methane Reforming of Supported Rh Nanoparticles. *J. Catal.* **2011**, *280*, 206−220.

(5) Wei, J.; Iglesia, E. Structural Requirements and Reaction Pathways in Methane Activation and Chemical Conversion Catalyzed by Rhodium. *J. Catal.* **2004**, *225*, 116−127.

(6) Parmaliana, A.; Arena, F.; Frusteri, F.; Coluccia, S.; Marchese, L.; Martra, G.; Chuvilin, A. L. Magnesia-Supported Nickel Catalysts: Ii. Surface Properties and Reactivity in Methane Steam Reforming. *J. Catal.* **1993**, *141*, 34−47.

(7) Spencer, N. D.; Schoonmaker, R. C.; Somorjai, G. A. Iron Single Crystals as Ammonia Synthesis Catalysts: Effect of Surface Structure on Catalyst Activity. *J. Catal.* **1982**, *74*, 129−135.

(8) Honkala, K.; Hellman, A.; Remediakis, I. N.; Logadottir, A.; Carlsson, A.; Dahl, S.; Christensen, C. H.; Nørskov, J. K. Ammonia Synthesis from First-Principles Calculations. *Science* **2005**, *307*, 555−558.

(9) Karim, A. M.; Prasad, V.; Mpourmpakis, G.; Lonergan, W. W.; Frenkel, A. I.; Chen, J. G.; Vlachos, D. G. Correlating Particle Size and Shape of Supported Ru/Γ-Al2o3 Catalysts with Nh3 Decomposition Activity. *J. Am. Chem. Soc.* **2009**, *131*, 12230−12239.

(10) Dahl, S.; Logadottir, A.; Egeberg, R. C.; Larsen, J. H.; Chorkendorff, I.; Törnqvist, E.; Nørskov, J. K. Role of Steps in N2 Activation on Ru(0001). *Phys. Rev. Lett.* **1999**, *83*, 1814−1817.

(11) Bezemer, G. L.; Bitter, J. H.; Kuipers, H. P. C. E.; Oosterbeek, H.; Holewijn, J. E.; Xu, X.; Kapteijn, F.; van Dillen, A. J.; de Jong, K. P. Cobalt Particle Size Effects in the Fischer−Tropsch Reaction Studied with Carbon Nanofiber Supported Catalysts. *J. Am. Chem. Soc.* **2006**, *128*, 3956−3964.

(12) Kang, J.; Zhang, S.; Zhang, Q.; Wang, Y. Ruthenium Nanoparticles Supported on Carbon Nanotubes as Efficient Catalysts for Selective Conversion of Synthesis Gas to Diesel Fuel. *Angew. Chem., Int. Ed.* **2009**, *48*, 2565−2568.

(13) Carballo, J. M. G.; Yang, J.; Holmen, A.; García-Rodríguez, S.; Rojas, S.; Ojeda, M.; Fierro, J. L. G. Catalytic Effects of Ruthenium Particle Size on the Fischer−Tropsch Synthesis. *J. Catal.* **2011**, *284*, 102−108.

(14) den Breejen, J. P.; Radstake, P. B.; Bezemer, G. L.; Bitter, J. H.; Frøseth, V.; Holmen, A.; de Jong, K. P. On the Origin of the Cobalt Particle Size Effects in Fischer−Tropsch Catalysis. *J. Am. Chem. Soc.* **2009**, *131*, 7197−7203.

(15) Iglesia, E.; Soled, S. L.; Fiato, R. A. Fischer-Tropsch Synthesis on Cobalt and Ruthenium. Metal Dispersion and Support Effects on Reaction Rate and Selectivity. *J. Catal.* **1992**, *137*, 212−224.

(16) Tuxen, A.; et al. Size-Dependent Dissociation of Carbon Monoxide on Cobalt Nanoparticles. *J. Am. Chem. Soc.* **2013**, *135*, 2273−2278.

(17) Van Santen, R. A. Complementary Structure Sensitive and Insensitive Catalytic Relationships. *Acc. Chem. Res.* **2009**, *42*, 57−66.

(18) Vendelbo, S. B.; Johansson, M.; Nielsen, J. H.; Chorkendorff, I. Is the Methanation Reaction over Ru Single Crystals Structure Dependent? *Phys. Chem. Chem. Phys.* **2011**, *13*, 4486−4493.

(19) Strebel, C.; Murphy, S.; Nielsen, R. M.; Nielsen, J. H.; Chorkendorff, I. Probing the Active Sites for Co Dissociation on Ruthenium Nanoparticles. *Phys. Chem. Chem. Phys.* **2012**, *14*, 8005−8012.

(20) van Etten, M. P. C.; Zijlstra, B.; Hensen, E. J. M.; Filot, I. A. W. Enumerating Active Sites on Metal Nanoparticles: Understanding the Size Dependence of Cobalt Particles for Co Dissociation. *ACS Catal.* **2021**, *11*, 8484−8492.

(21) Agrawal, R.; Phatak, P.; Spanu, L. Effect of Phase and Size on Surface Sites in Cobalt Nanoparticles. *Catal. Today* **2018**, *312*, 174−180.

(22) Rahm, J. M.; Erhart, P. Beyond Magic Numbers: Atomic Scale Equilibrium Nanoparticle Shapes for Any Size. *Nano Lett.* **2017**, *17*, 5775−5781.

(23) van Helden, P.; Ciobîcă, I. M.; Coetzer, R. L. J. The Size-Dependent Site Composition of Fcc Cobalt Nanocrystals. *Catal. Today* **2016**, *261*, 48−59.

(24) Claeys, M.; Van Steen, E. Basic studies. *Stud. Surf. Sci. Catal.* **2004**, *152*, 601−680.

(25) Saib, A. M.; Borgna, A.; van de Loosdrecht, J.; van Berge, P. J.; Niemantsverdriet, J. W. In situ surface oxidation study of a planar Co/SiO2/Si(100) model catalyst with nanosized cobalt crystallites under model Fischer-Tropsch synthesis conditions. *J. Phys. Chem. B* **2006**, *110*, 8657−8664.

(26) Bruix, A.; Margraf, J. T.; Andersen, M.; Reuter, K. First-Principles-Based Multiscale Modelling of Heterogeneous Catalysis. *Nat. Catal.* **2019**, *2*, 659−670.

(27) Senftle, T. P.; et al. The Reaxff Reactive Force-Field: Development Applications and Future Directions. *npj Comput. Mater.* **2016**, *2*, 15011.

(28) Fröhlking, T.; Bernetti, M.; Calonaci, N.; Bussi, G. Toward Empirical Force Fields That Match Experimental Observables. *J. Chem. Phys.* **2020**, *152*, 230902.

(29) van de Loosdrecht, J.; Botes, F. G.; Ciobica, I. M.; Ferreira, A.; Gibson, P.; Moodley, D. J.; Saib, A. M.; Visagie, J. L.; Weststrate, C. J.; Niemantsverdriet, J. W. Fischer−Tropsch Synthesis: Catalysts and Chemistry. In *Comprehensive Inorganic Chemistry II*, 2nd edition; Reedijk, J.; Poeppelmeier, K., Eds.; Elsevier: Amsterdam, 2013; pp 525−557.

(30) Oukaci, R.; Singleton, A. H.; Goodwin, J. G. Comparison of Patented Co F−T Catalysts Using Fixed-Bed and Slurry Bubble Column Reactors. *Appl. Catal., A* **1999**, *186*, 129−144.

(31) Warayanon, W.; Tungkamani, S.; Sukkathanyawat, H.; Phongaksorn, M.; Ratana, T.; Sornchamni, T. Effect of Manganese Promoter on Cobalt Supported Magnesia Catalyst for Fischer-Tropsch Synthesis. *Energy Procedia* **2015**, *79*, 163−168.

(32) Zhang, Y.; Xiong, H.; Liew, K.; Li, J. Effect of Magnesia on Alumina-Supported Cobalt Fischer−Tropsch Synthesis Catalysts. *J. Mol. Catal. A: Chem.* **2005**, *237*, 172−181.

(33) Parastaev, A.; Muravev, V.; Huertas Osta, E.; van Hoof, A. J. F.; Kimpel, T. F.; Kosinov, N.; Hensen, E. J. M. Boosting Co2

Hydrogenation Via Size-Dependent Metal−Support Interactions in Cobalt/Ceria-Based Catalysts. *Nat. Catal.* **2020**, *3*, 526−533.
(34) Deng, K.; Lin, L.; Rui, N.; Vovchok, D.; Zhang, F.; Zhang, S.; Senanayake, S. D.; Kim, T.; Rodriguez, J. A. Studies of Co2 Hydrogenation over Cobalt/Ceria Catalysts with in Situ Characterization: The Effect of Cobalt Loading and Metal−Support Interactions on the Catalytic Activity. *Catal. Sci. Technol.* **2020**, *10*, 6468−6482.
(35) Munirathinam, R.; Pham Minh, D.; Nzihou, A. Effect of the Support and Its Surface Modifications in Cobalt-Based Fischer−Tropsch Synthesis. *Ind. Eng. Chem. Res.* **2018**, *57*, 16137−16161.
(36) van Deelen, T. W.; Hernández Mejía, C.; de Jong, K. P. Control of Metal-Support Interactions in Heterogeneous Catalysts to Enhance Activity and Selectivity. *Nat. Catal.* **2019**, *2*, 955−970.
(37) Pestman, R.; Chen, W.; Hensen, E. Insight into the Rate-Determining Step and Active Sites in the Fischer−Tropsch Reaction over Cobalt Catalysts. *ACS Catal.* **2019**, *9*, 4189−4195.
(38) van Duin, A. C. T.; Dasgupta, S.; Lorant, F.; Goddard, W. A. Reaxff: A Reactive Force Field for Hydrocarbons. *J. Phys. Chem. A* **2001**, *105*, 9396−9409.
(39) Chenoweth, K.; van Duin, A. C. T.; Goddard, W. A. Reaxff Reactive Force Field for Molecular Dynamics Simulations of Hydrocarbon Oxidation. *J. Phys. Chem. A* **2008**, *112*, 1040−1053.
(40) AMS 2023.1, SCM, Theoretical Chemistry, Vrije Universiteit, Amsterdam, The Netherlands, http://www.scm.com.
(41) Matsumoto, M.; Nishimura, T. Mersenne Twister: A 623-Dimensionally Equidistributed Uniform Pseudo-Random Number Generator. *ACM Trans. Model. Comput. Simul.* **1998**, *8*, 3−30.
(42) Cheula, R.; Soon, A.; Maestri, M. Prediction of Morphological Changes of Catalyst Materials under Reaction Conditions by Combined Ab Initio Thermodynamics and Microkinetic Modelling. *Catal. Sci. Technol.* **2018**, *8*, 3493−3503.
(43) Karaca, H.; Hong, J.; Fongarland, P.; Roussel, P.; Griboval-Constant, A.; Lacroix, M.; Hortmann, K.; Safonova, O. V.; Khodakov, A. Y. In Situ Xrd Investigation of the Evolution of Alumina-Supported Cobalt Catalysts under Realistic Conditions of Fischer-Tropsch Synthesis. *Chem. Commun.* **2010**, *46*, 788−790.
(44) Kresse, G.; Furthmüller, J. Efficiency of Ab-Initio Total Energy Calculations for Metals and Semiconductors Using a Plane-Wave Basis Set. *Comput. Mater. Sci.* **1996**, *6*, 15−50.
(45) Kresse, G.; Furthmüller, J. Efficient Iterative Schemes for Ab Initio Total-Energy Calculations Using a Plane-Wave Basis Set. *Phys. Rev. B* **1996**, *54*, 11169−11186.
(46) Kresse, G.; Hafner, J. Ab Initio Molecular Dynamics for Liquid Metals. *Phys. Rev. B* **1993**, *47*, 558−561.
(47) Kresse, G.; Joubert, D. From Ultrasoft Pseudopotentials to the Projector Augmented-Wave Method. *Phys. Rev. B* **1999**, *59*, 1758−1775.
(48) Perdew, J. P.; Burke, K.; Ernzerhof, M. Generalized Gradient Approximation Made Simple. *Phys. Rev. Lett.* **1996**, *77*, 3865−3868.
(49) Methfessel, M.; Paxton, A. T. High-Precision Sampling for Brillouin-Zone Integration in Metals. *Phys. Rev. B* **1989**, *40*, 3616−3621.
(50) Geysermans, P.; Finocchi, F.; Goniakowski, J.; Hacquart, R.; Jupille, J. Combination of (100), (110) and (111) Facets in Mgo Crystals Shapes from Dry to Wet Environment. *Phys. Chem. Chem. Phys.* **2009**, *11*, 2228−2233.
(51) Du, Z.; de Leeuw, N. H. A Combined Density Functional Theory and Interatomic Potential-Based Simulation Study of the Hydration of Nano-Particulate Silicate Surfaces. *Surf. Sci.* **2004**, *554*, 193−210.
(52) Lazzeri, M.; Vittadini, A.; Selloni, A. Structure and Energetics of Stoichiometric Tio2 Anatase Surfaces. *Phys. Rev. B* **2001**, *63*, No. 155409.
(53) Digne, M.; Sautet, P.; Raybaud, P.; Euzen, P.; Toulhoat, H. Hydroxyl Groups on Γ-Alumina Surfaces: A Dft Study. *J. Catal.* **2002**, *211*, 1−5.
(54) Esch, F.; Fabris, S.; Zhou, L.; Montini, T.; Africh, C.; Fornasiero, P.; Comelli, G.; Rosei, R. Electron Localization Determines Defect Formation on Ceria Substrates. *Science* **2005**, *309*, 752−755.
(55) Das, T.; Deo, G. Effects of Metal Loading and Support for Supported Cobalt Catalyst. *Catal. Today* **2012**, *198*, 116−124.
(56) Reinhart, W. F.; Long, A. W.; Howard, M. P.; Ferguson, A. L.; Panagiotopoulos, A. Z. Machine Learning for Autonomous Crystal Structure Identification. *Soft Matter* **2017**, *13*, 4733−4745.
(57) Filot, I. A. W.; van Etten, M. P. C.; Trommelen, D.; Hensen, E. J. M. Bramble: adaptive common neighbor analysis (CNA) for the recognition of surface topologies in nanoparticles (v1.0.0). *Zenodo* **2023**, DOI: 10.5281/zenodo.8129268.
(58) Kitakami, O.; Sato, H.; Shimada, Y.; Sato, F.; Tanaka, M. Size Effect on the Crystal Phase of Cobalt Fine Particles. *Phys. Rev. B* **1997**, *56*, 13849−13854.